Frequency-Directivity Scanning in Laboratory Radar Imaging

Jacqueline Bertrand

CNRS and University Paris VII, LPTM, 75251 Paris, France

Pierre Bertrand and Jean-Philippe Ovarlez

ONERA/DES, BP 72, 92322 Chatillon, France

ABSTRACT

This work concerns an extension of usual radar imaging in which the pictures of the target do not simply exhibit the position of elementary reflectors but also give the behavior of these reflectors when the frequency and the direction of illumination vary. Essentially, the technique consists of describing the target by a generalized image which can be computed from the knowledge of the backscattering function on a large domain in the angle-frequency space. A discussion of the physical relevance of the approach is given and its conclusions are used to derive a practical formulation relying on a special wavelet transform. The implementation of the technique is developed by using the fast Mellin transform. Special features of the method are the use of data in polar format without resampling and the fact that the computation can be easily parallelized.

I. INTRODUCTION

Radar imaging is a special technique of microwave imaging in which the computed pictures correspond to maps of elementary reflectors [1]. It works by processing scattering data collected by a coherent radar system. The basic assumption of the operation is that the contribution of multiple reflections on the target can be neglected.

The problem addressed here concerns operations of monostatic type which are confined to the laboratory and the anechoic chamber. The observed targets are finite objects whose backscattering coefficients can effectively be measured for various frequencies and directions of observation. The object of the imaging operation is then to extract information on the location of the main reflecting parts of these targets.

In practice, the question of the vectorial nature of the electromagnetic field cannot be avoided and it will be solved by fixing the polarizations of the emitting and receiving antennas. Such an experimental procedure is unambiguous as long as the changes in the direction of illumination correspond to a rotation of the target around an axis perpendicular to the radar line of sight. In that case, the data collected are samples of a complex-valued function depending on the emitted frequency f and on the target orientation θ. For convenience, this function will be noted $H(\mathbf{k})$, where $\mathbf{k}$ is a two-dimensional vector corresponding to the point of polar coordinates $(2f/c, \theta)$, c being the velocity of light. It can be noted that any imaging operation working with the above set of data will permit one only to localize the projections of the bright points on the measurement plane.

In classical radar imaging the backscattering coefficient $H(\mathbf{k})$ is supposed to be acquired on some frequency band $(f_{\min}, f_{\max})$ and on some angular sector $(\theta_{\min}, \theta_{\max})$ and the image is obtained either by a range-Doppler analysis [2] or by a bidimensional Fourier transform [3]. The two classical procedures provide useful results but they both introduce computational difficulties due to the fact that their algorithms cannot work efficiently with data collected in polar format.

Great progress in the experimental techniques has permitted the coherent measurement of the backscattering coefficient over wide frequency bands (for example, from 2 to 18 Ghz or more) and this for all values of angle. As a result, many images of the same target can be computed by processing the samples contained in various windows corresponding to subsectors and subbands of the observation domain. Such images are naturally labeled by the mean frequency and the mean orientation of the target and their study displays the evolution of the bright points in a change of the scattering parameters. The systematic exploitation of this possibility is what we call a frequency-directivity scanning operation.

Actually, laboratory radar imaging procedures can be reformulated by introducing from the start the concept of spectral image which consists of describing the target by a distribution $R(\mathbf{x}, \mathbf{k})$ of bright points located in $\mathbf{x}$ and reflecting in the direction of $\mathbf{k}$ for the frequency $c|\mathbf{k}|/2$. In this approach, the whole set of classical images corresponding to various $\mathbf{k}$ is treated as a unique hyperimage in four-dimensional space $(\mathbf{x}, \mathbf{k})$. The operation is licit provided some consistency constraint is verified in order to ensure the physical relevance of the description. Basically, the essential requirement is that different observers, using different reference frames and different measuring scales in the laboratory, be able to compare their results, i.e., the spectral images they have formed. Since reference systems are connected by translations, rotations, and scalings, the fundamental role in the analytical formulation of the constraint is played by the similarity group of the plane which consists exactly of these transformations. The object of the following developments is

Manuscript received 29 July 1993; revised manuscript received 8 December 1993

CCC 0899-9457/94/010039-13

to show how the above remarks can be exploited to derive a practical expression of the spectral image.

In Sec. II the definition of the backscattering coefficient $H(\mathbf{k})$ is recalled and its transformation in a change of reference frame is derived. The fundamental constraint of covariance is then written as a relation between the transformation rules which apply to the backscattering coefficient and to the spectral image respectively. These preliminaries are used in Sec. III to express the spectral image $R(\mathbf{x}, \mathbf{k})$ in terms of a continuous wavelet transform of the backscattering function $H(\mathbf{k})$. This approach is completed in Sec. IV by an original computational technique which is essentially founded on the use of a Mellin transform which respect to the frequency variable. The algorithm works directly on samples in polar format and, if needed, its structure could be easily parallelized. Finally, practical applications are presented in Sec. V. These applications deal with numerical simulations and some examples of results obtained with a real target.

II. ANALYTICAL FRAME

A. Radar Backscattering Coefficient. Despite its familiarity, the notion of the backscattering coefficient is essentially a theoretical one and its experimental characterization deserves great attention. However, as long as we are only concerned with the imaging technique, it is sufficient to recall the formal aspect of the subject and to suppose that all useful data can be acquired in the laboratory. As specified in the Introduction, we will only consider planar measurements in which the values of the backscattering coefficients are obtained by rotating the target around some axis perpendicular to the radar line of sight.

Suppose that the radar is at distance D from a point O chosen on the target or in its vicinity and that the impinging field E_I is a plane wave whose wave vector points in the direction of O. If the observation distance D is much greater than the size of the target, the scattered field E_S received by the radar has approximately the form of a spherical wave issued from O. Moreover, for a static target, this field is reradiated without change of frequency. At this point a simplification occurs when the polarizations of the emitting and receiving antennas are fixed. In this case, the observable effect of the target is simply described by the ratio E_S/E_I of two complex numbers representing the values of the incoming and outgoing fields at the radar. This leads to a definition of the radar backscattering coefficient through a limit operation:

$$H(f, \theta) = \lim_{D \to \infty} \sqrt{4\pi} D \, \frac{E_S}{E_I} \, e^{4i\pi f D/c} . \tag{1}$$

In this formula, the variable θ specifies the direction of observation in the measurement plane and c is the velocity of light. The explicit form of (1) supposes that the time dependence of the fields is of the form $e^{2i\pi ft}$. When the measurement radius D increases, the modulus of E_S/E_I goes to zero while its phase grows without limit. This observation explains the introduction of D-dependent corrective factors in (1) in order that a finite limit be obtained. In particular, the exponential factor $e^{4i\pi fD/c}$ ensures that the argument of the limit corresponds to the phase that the ratio E_S/E_I would have at the center of measurement O. As a result the backscattering coefficient (1) is not only representative of the target but also of the choice of the point O, which is called "origin of phases." In an actual experiment, this point is in fact determined by the calibration process.

In the following, the two variables of the backscattering coefficient will be described by a vector $\mathbf{k}$ with polar components $k = 2f/c$ and θ. With this notation, the effect of a translation $\mathbf{OO}'$ of the origin of the phases is expressed by

$$H(\mathbf{k}) \to H'(\mathbf{k}) = H(\mathbf{k}) e^{-2i\pi \mathbf{k} \cdot \mathbf{OO}'} . \tag{2}$$

B. Spectral Image and Similarity Group. The complex function introduced by the mathematical definition (1) completely characterizes the scattering process in a monostatic radar experiment involving specific polarizations. This function does not have a direct physical interpretation but it can be used to build real-valued expressions of practical interest. A very common example of this fact is given by the radar cross section which is of the form

$$\sigma(\mathbf{k}) = |H(\mathbf{k})|^2 . \tag{3}$$

This quantity is insensitive to a displacement of the origin of phases [cf. (2)] and is considered as the main scattering characteristic in quantum physics (and in classical optics) where the phase of the backscattering coefficient is generally unknown. In the radar context, it gives information on the frequency-directivity of the reflecting parts of the target but nothing on their positions.

In modern radar experiments, the whole measurement of (1) is possible and this fact supports the idea of seeking alternative descriptions that give information not only on the frequency-directivity $\mathbf{k}$ of the bright points but also on their position $\mathbf{x}$. Analytically this suggests to generalize (3) by a relation such as

$$R(\mathbf{x}, \mathbf{k}) = \int K(\mathbf{k}_1, \mathbf{k}_2, \mathbf{x}, \mathbf{k}) H(\mathbf{k}_1) H^*(\mathbf{k}_2) \, d\mathbf{k}_1 \, d\mathbf{k}_2 , \tag{4}$$

where R represents a spectral image of the target and where the kernel K is supposed to be Hermitian.

In fact, the form of the kernel can be specified by using some more physical arguments relative to the interpretation of the image we are seeking. The essential constraint is the invariance of relation (4) by a change of observer, i.e., by a change of reference system.

According to the experimental situation, a change of reference system is essentially a change of origin, axis orientation, and scale of length in the plane of measurements. However, for a complete description of the operation, two tacit agreements between observers have to be added. The first one is that any change of length scale be accompanied by a proportional change of time scale so that the value of the velocity of light is conserved. The second one concerns the experimental practice and consists in admitting that the origin of phases coincides for each observer with the origin of coordinates.

The coordinates $(\mathbf{x}, t)$ and $(\mathbf{x}', t')$ of a point for two different observers are related in the following way:

$$\begin{aligned} \mathbf{x} &\to \mathbf{x}' = a\mathcal{R}_\phi \mathbf{x} + \mathbf{b} , \\ t &\to t' = at , \end{aligned} \tag{5}$$

where the two-vector $\mathbf{b}$ characterizes the change of origin of the reference system, $\mathcal{R}_\phi$ its rotation by angle ϕ and $a>0$ the dilation in length and time. The coordinates $\mathbf{k}$ are transformed accordingly as

$$\mathbf{k} \rightarrow \mathbf{k}' = a^{-1}\mathcal{R}_\phi \mathbf{k} \tag{6}$$

since frequency transforms as the inverse of time.

Recalling the definition of the backscattering coefficient $H(\mathbf{k})$ and using the agreement between observers on the choice of the origin of phases, we are able to write the transformation law of H in a change of reference systems defined by (5) and (6):

$$H(\mathbf{k}) \rightarrow H'(\mathbf{k}) = a e^{-2i\pi \mathbf{k}\cdot\mathbf{b}} H(a\mathcal{R}_\phi^{-1}\mathbf{k}) . \tag{7}$$

The a factor in front is there to ensure that H transforms as a length in a dilation as it should since $|H|^2$ is a cross section. The usual inner product on functions H is given by

$$(H_1, H_2) = \int_0^{2\pi} d\theta \int_0^\infty H_1(k,\theta) H_2^*(k,\theta) k\, dk \tag{8}$$

and is easily seen to be invariant under transformation (7). As a matter of fact, this property is a special feature of the two-dimensional case. In problems with a different number of dimensions, the scalar product invariant by the transformation (7) of H will not be the usual one: an adequate power of k will appear as a weight in the integration [4].

In a change of reference frame, distribution $R(\mathbf{x},\mathbf{k})$ is required to transform pointwise as a dimensionless quantity:

$$R(\mathbf{x},\mathbf{k}) \rightarrow R'(\mathbf{x},\mathbf{k}) = R(a^{-1}\mathcal{R}_{-\phi}(\mathbf{x}-\mathbf{b}), a\mathcal{R}_{-\phi}\mathbf{k}) . \tag{9}$$

In this way, the integral

$$S_{\mathcal{D}}(\mathbf{k}) = \int_{\mathcal{D}} R(\mathbf{x},\mathbf{k})\, d\mathbf{x} \tag{10}$$

on some domain $\mathcal{D}$ of the measurement plane has the dimension of a surface and can in fact be interpreted as that part of the scattering cross section due to the elements of the target with projections in $\mathcal{D}$.

Constraints considered so far are not sufficient to determine $R(\mathbf{x},\mathbf{k})$ uniquely. The solution that will be studied relies on a continuous wavelet analysis associated with the similarity group of the plane.

III. WAVELET FORMULATION OF THE PROBLEM

A. Analysis of the Backscattering Coefficient. The principle of continuous wavelet analysis [5–8] will first be recalled to fix notations in the two-dimensional case and emphasize the relationship between the space $(\mathbf{x},\mathbf{k})$ and the similarity group.

Let $\Phi(\mathbf{k})$ be a basic wavelet supposed to represent the backscattering coefficient of a template target which would be located about the point $\mathbf{x}=0$ and would reflect mainly in the direction of $\theta=0$ at a frequency characterized by $k \equiv 2f/c = 1$. By convention Φ is thus attached to the point P_0 defined by the coordinates

$$\mathbf{x}=0 , \quad \mathbf{k} \equiv (k,\theta) = (1,\theta) . \tag{11}$$

In a similarity transformation $(a, \mathcal{R}_\phi, \mathbf{b})$ point P_0 goes into a point P whose coordinates are given by

$$\mathbf{x} = \mathbf{b} , \quad \mathbf{k} \equiv (k,\theta) = (a^{-1}, \phi) . \tag{12}$$

Simultaneously wavelet Φ is transformed according to (7) and, due to relation (12), is seen to be attached to point P. Its explicit expression is

$$\Phi_{\mathbf{x}\mathbf{k}}(k') = k^{-1} e^{-2i\pi \mathbf{k}'\cdot\mathbf{x}} \Phi\left(\frac{k'}{k}, \theta' - \theta\right) . \tag{13}$$

The family of wavelets thus obtained for all similarity transformations constitutes a set of basis functions that will be the same in all reference frames. Indeed, because of the group property, a change of observer will simply be expressed by a change in the labeling of family (13).

The wavelet coefficient $C(\mathbf{x},\mathbf{k})$ associated with H is defined as usual by the scalar product of H and the wavelet

$$C(\mathbf{x},\mathbf{k}) = (H, \Phi_{\mathbf{x}\mathbf{k}}) \tag{14}$$

or according to (8)

$$C(\mathbf{x},\mathbf{k}) = \int_0^{2\pi} d\theta' \int_0^\infty dk' \frac{k'}{k} H(k',\theta') e^{2i\pi \mathbf{k}'\cdot\mathbf{x}} \Phi^*\left(\frac{k'}{k}, \theta' - \theta\right) . \tag{15}$$

The squared modulus of C integrated over the whole $(\mathbf{x},\mathbf{k})$ space is given by

$$\begin{aligned}\int_{R^3\times R^3} |C(\mathbf{x},\mathbf{k})|^2\, d\mathbf{x}\, d\mathbf{k} \equiv \int & H(\mathbf{k}') H^*(\mathbf{k}'') e^{2i\pi(\mathbf{k}'-\mathbf{k}'')\cdot\mathbf{x}} \\ & \times \Phi^*\left(\frac{k'}{k}, \theta' - \theta\right) \Phi\left(\frac{k''}{k}, \theta'' - \theta\right) \\ & \times d\mathbf{k}'\, d\mathbf{k}''\, d\mathbf{x}\, \frac{d\mathbf{k}}{k^2}\end{aligned} \tag{16}$$

or, after performing the $\mathbf{x}$ and $\mathbf{k}''$ integrals,

$$\begin{aligned}&\int_{R^3\times R^3} |C(\mathbf{x},\mathbf{k})|^2\, d\mathbf{x}\, d\mathbf{k} \\ &\quad = \int |H(k',\theta')|^2 \left|\Phi\left(\frac{k'}{k}, \theta' - \theta\right)\right|^2 d\mathbf{k}'\, \frac{d\mathbf{k}}{k^2} .\end{aligned} \tag{17}$$

A change of variables then leads to the so-called isometry formula:

$$\int |C(\mathbf{x},\mathbf{k})|^2\, d\mathbf{x}\, d\mathbf{k} = \|H\|^2 \chi(\Phi) \tag{18}$$

where the function χ depends only on the choice of the mother wavelet and is given by

$$\chi(\Phi) \equiv \int |\Phi(\mathbf{k})|^2 \frac{d\mathbf{k}}{k^2} . \tag{19}$$

For finiteness of (18), the wavelet Φ must satisfy the so-called admissibility condition $\chi < \infty$. In that case, formula (15) can be inverted, allowing the reconstruction of H from its wavelet

coefficient according to

$$H(\mathbf{k}) = \frac{1}{\chi(\Phi)} \int C(\mathbf{x}, \mathbf{k}) \Phi_{\mathbf{xk}}(\mathbf{k})\, d\mathbf{x}\, d\mathbf{k} . \tag{20}$$

B. Generation of a Spectral Image. The above wavelet scheme yields a possible candidate [4] for the spectral image that can be set equal to

$$R(\mathbf{x}, \mathbf{k}) = \frac{1}{\chi} |C(\mathbf{x}, \mathbf{k})|^2 , \tag{21}$$

where C is defined by (15). In this case the kernel in relation (4) has the following form:

$$K(\mathbf{k}_1, \mathbf{k}_2, \mathbf{x}, \mathbf{k}) = \frac{k_1 k_2}{\chi k^2} e^{2i\pi(\mathbf{k}_1 - \mathbf{k}_2)\cdot\mathbf{x}} \times \Phi^*\left(\frac{k_1}{k}, \theta_1 - \theta\right)\Phi\left(\frac{k_2}{k}, \theta_2 - \theta\right) . \tag{22}$$

This choice has several interesting features. The image so defined is a positive function which transforms as required in Section II under a change of observers. Namely, when a similarity transformation is applied to the backscattering coefficient H as in (7), the definition of the wavelet coefficient (14) implies that $R(\mathbf{x}, \mathbf{k})$ in (21) is transformed by (9) and the interpolation (10) holds. It is also possible to proceed further in computing the integral of $R(\mathbf{x}, \mathbf{k})$ over $\mathbf{x}$-space. This gives

$$\int R(\mathbf{x}, \mathbf{k})\, d\mathbf{x} = \int_0^{2\pi} d\theta' \int_0^{\infty} dk' k' |H(k', \theta')|^2 \chi^{-1} \frac{1}{k^2} \times \left|\Phi\left(\frac{k'}{k}, \theta' - \theta\right)\right|^2 . \tag{23}$$

The result is a smoothing of the radar cross section which depends on the spectral width of the basic wavelet and which commutes with the action of the similarity group. This implies that the $\mathbf{x}$ integral of R is transformed like a cross section in a similarity transformation and can thus be interpreted consistently by different observers. Moreover, if the mother wavelet Φ is made to shrink around the point $(k = 0, \theta = 0)$, the right-hand side of (23) will come closer and closer to $|H|^2$, thus featuring the behavior of $R(\mathbf{x}, \mathbf{k})$ as a spatial distribution of bright points characterized by $\mathbf{k}$. However, in this process, the wavelet spreads out in $\mathbf{x}$ space and all information on the position of the points is lost. This tradeoff between $\mathbf{x}$ and $\mathbf{k}$ localization is inherent to the problem and will be discussed in Section V.

All these remarks strongly support the choice of (21) as a definition of the spectral image. In the formulation, the inescapable fuzziness due to the uncertainty relations is controlled by the choice of the mother wavelet Φ.

IV. IMPLEMENTATION TECHNIQUES

A. Interest of the Mellin Transform. Samples of the backscattering coefficient H are obtained experimentally in polar coordinates k,θ and the straightforward computation of the wavelet coefficient defined by (15) requires to change from polar to Cartesian coordinates before performing a two-dimensional Fourier transform. However, such operations are very costly as they rely heavily on resampling, first to obtain Cartesian samples of H and then to perform dilations of the wavelet in (15). Here instead, we propose a computation which can be performed directly in polar coordinates provided that the sampling of the backscattering function corresponds to regularly spaced angles and geometrically spaced frequencies.

The definition, properties, and discretization of the Mellin transform relevant to signal analysis have been recalled in the Appendix. The present application corresponds to the special case $r = 0$.

The Mellin transform of the backscattering function with respect to k is defined by

$$\mathcal{M}[H](\beta, \theta) = \int_0^{\infty} H(k, \theta) k^{2i\pi\beta}\, dk \tag{24}$$

and satisfies a Parseval formula given by

$$\int_0^{\infty} H_1(k, \theta) H_2^*(k, \theta) k\, dk = \int_{-\infty}^{\infty} \mathcal{M}[H_1](\beta, \theta) \times \mathcal{M}^*[H_2](\beta, \theta)\, d\beta . \tag{25}$$

To apply these formulas to the computation of the wavelet coefficient, define the functions $\tilde{H}$ and $\tilde{\Phi}$ by

$$\tilde{H}(\mathbf{k}') = H(\mathbf{k}') e^{2i\pi\mathbf{k}'\cdot\mathbf{x}} , \tag{26}$$

$$\tilde{\Phi}(\mathbf{k}') = \frac{1}{k} \Phi\left(\frac{k'}{k}, \theta'\right) . \tag{27}$$

Then (15) becomes

$$C(\mathbf{x}, \mathbf{k}) = \int_0^{2\pi} d\theta' \int_{-\infty}^{\infty} d\beta\, \mathcal{M}[\tilde{H}](\beta, \theta') \mathcal{M}^*[\tilde{\Phi}](\beta, \theta' - \theta) . \tag{28}$$

Property (52) of the Mellin transform implies

$$\mathcal{M}[\tilde{\Phi}](\beta, \theta') = k^{2i\pi\beta} \mathcal{M}[\Phi](\beta, \theta') . \tag{29}$$

Finally, introducing the Fourier coefficients of functions $\mathcal{M}[\tilde{H}](\beta, \theta')$ and $\mathcal{M}[\Phi](\beta, \theta')$ according to the formula

$$\hat{\mathcal{M}}_n[\tilde{H}](\beta) = \frac{1}{2\pi} \int_0^{2\pi} \mathcal{M}[\tilde{H}](\beta, \theta') e^{-in\theta'}\, d\theta' , \tag{30}$$

we are able to rewrite the expression of the wavelet coefficient as

$$C(\mathbf{x}, \mathbf{k}) = \sum_n \int_{-\infty}^{\infty} d\beta\, \hat{\mathcal{M}}_n[\tilde{H}](\beta) \hat{\mathcal{M}}_n^*[\Phi](\beta) e^{in\theta} k^{-2i\pi\beta} . \tag{31}$$

In this form, the computation of the wavelet coefficient reduces to Fourier and Mellin transforms which can all be performed by a fast Fourier transform (FFT) algorithm. First, the Mellin and Fourier transforms $\hat{\mathcal{M}}_n[\Phi](\beta)$ of the basis wavelet Φ is obtained once and for all by two FFTs. Then, for each position $\mathbf{x}$ of the bright points, the Mellin and Fourier transforms $\hat{\mathcal{M}}_n[\tilde{H}](\beta)$ of $H(\mathbf{k}) e^{2i\pi\mathbf{k}\cdot\mathbf{x}}$ are computed, also using two FFTs. Finally, two inverse FFTs yield the dependence of C on angle θ and frequency k. The whole process can be done all over for different values of position $\mathbf{x}$.

B. Rules of Sampling. In any practical situation, the limited extension of $H(k, \theta)$ in k and the finite size of the target imply that, for a reasonable wavelet, the support of coefficient C will also be limited in (**x**,**k**) space. A more thorough description of this space is provided by the affine time-frequency distribution [9, 10] reinterpreted as an (x, k) distribution $P(x, k)$: it associates hyperbolas $x = x_0 + \beta/k$ with signals $k^{-1-2i\pi\beta}e^{-i\pi x_0 k}$ of the Mellin "basis." In this way the β Mellin variable gets an interpretation in (**x**, **k**) space which allows one to determine directly the support of $\mathcal{M}(\beta, \theta)$. Namely, if H is zero outside the interval $[k_1, k_2]$ and if the maximum length of the target in any direction is L, distribution P is approximately equal to zero outside the shaded region displayed on Fig. 1. From there it can be shown that the extreme values of the support $(\beta, -\beta)$ of $\mathcal{M}(\beta, \theta)$ correspond to the β labels of the hyperbolas limiting the region. According to Fig. 1, this is given by

$$\beta = k_2 L/2 . \tag{32}$$

Coefficient C can now be computed according to (31). First, for a given θ, choose N_k samples of H geometrically spaced in the following way:

$$H(n, \theta) = H(k_1 Q^{n/N_k}, \theta) , \quad 0 \le n < N_k , \tag{33}$$

where

$$Q = k_2/k_1 . \tag{34}$$

As seen in Sec. A.2 [Eqs. (A21) and (A24)], computation of the discrete Mellin transform of H requires that the number N_k of samples be such that

$$\frac{N_k}{\ln Q} > 2\beta . \tag{35}$$

Relations (32) and (34) then lead to the condition that must be satisfied by the number of samples in the k domain to avoid aliasing. With the relation $k = 2f/c$, this condition can be written directly in terms of frequencies as

$$N_k > 2 f_2 \ln(f_2/f_1) L/c . \tag{36}$$

Integration on the θ variable reduces to a discrete Fourier transform which is performed in the usual way. This leads to choose N_θ samples such that

$$N_\theta > 2\,\Delta\theta f_2 L/c , \tag{37}$$

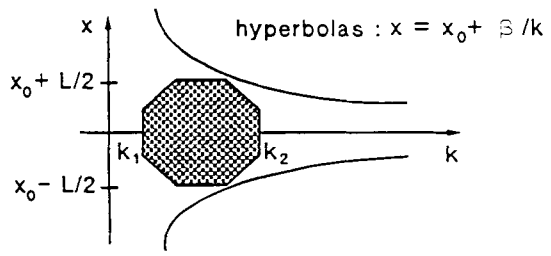

Figure 1. Determination of the β extent for a target with maximal length L located around x_0 and analyzed on $[k_1, k_2]$.

where $\Delta\theta$ represents the range of θ for which the coefficient H is different from zero.

In conclusion, the N_f useful frequency samples must be chosen geometrically spaced and verifying condition (36) while the N_θ angular samples must be regularly spaced in the usual way, as shown in Fig. 2. The computation is then performed directly with these samples of the backscattering coefficient.

Let N_x and N_y denote the number of points in range and cross-range space, respectively. The complexity of the algorithm is given by

$$N_x N_y[(2N_\theta + 1) \text{ FFT of } N_f \text{ points} + (2N_f + 1) \text{ FFT of } N_\theta \text{ points}]$$

for a number $N_f N_\theta$ of computed radar images.

V. APPLICATION TO PRACTICAL SITUATIONS

In each application, the resolution of the images in **x** space will depend on the choice of the basic wavelet. To guide this choice, we will first study how these resolutions are related to the spread of the wavelet in **k** space.

A. Interrelations of the Resolutions. Suppose the analyzed domain in (k, θ) space is centered at $(k = k_0, \theta = \theta_0)$ and spreads out on a band Δk and an angular width $\Delta\theta$. Choosing as basic wavelet Φ the characteristic function of the domain $1 - \Delta k/2 < k < 1 + \Delta k/2$, $-\Delta\theta/2 < \theta < \Delta\theta/2$, we obtain the following expression for the wavelet coefficient (15) computed at point $(k = k_0, \theta = \theta_0)$:

$$C(\mathbf{x}, k_0, \theta_0) = \int_{k_0(1-\Delta k/2)}^{k_0(1+\Delta k/2)} \int_{\theta_0 - \Delta\theta/2}^{\theta_0 + \Delta\theta/2} H(k', \theta') \times e^{2i\pi k'[x_0 \cos(\theta' - \theta_0) + y_0 \sin(\theta' - \theta_0)]} \times \frac{k'}{k_0}\, dk'\, d\theta' , \tag{38}$$

where (x_0, y_0) are the coordinates of **x** in a frame rotated by θ_0.

It is interesting to note that (38) is nothing but the classical formulation of two-dimensional radar imaging [3].

Under the small-$\Delta\theta$ assumptions, $\sin(\theta' - \theta_0) \approx \theta' - \theta_0$,

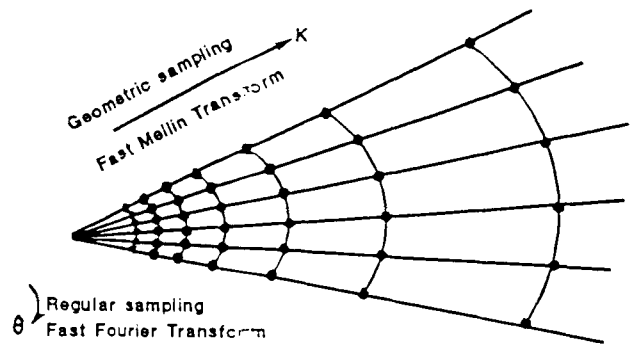

Figure 2. Sampling mode of the backscattering coefficient. The frequency samples are collected in geometrical progression on the analysis frequency bandwidth while the angular samples are collected in the classical way.

$\cos(\theta' - \theta_0) \approx 1$, and the coefficient (38) can be approximated as

$$C(\mathbf{x}, k_0, \theta_0) = \int_{k_0(1+\Delta k/2)}^{k_0(1+\Delta k/2)} \left(\int_{-\Delta\theta/2}^{\Delta\theta/2} H(k', \theta' + \theta_0) e^{2i\pi k' y_0 \theta'} \, d\theta' \right) \times e^{2i\pi k' x_0} \frac{k'}{k} \, dk' . \quad (39)$$

The interrelation between θ and x variables has completely disappeared and the range resolution thus depends only on the bandwidth. Besides, the resolution in the product ky_0 is directly related to the resolution in variable θ.

The classical method to compute the expression of C given by (39) is to perform the discrete Fourier transform on the frequency (dual variable x_0) and angular variables (dual variable $ky = 2fy_0/c$). This method is interesting in terms of the number of operations to perform. Nevertheless, this technique must generally be followed by a resampling in cross-range space due to the frequency dependence of the result.

If we denote by $L_{\max}$ the maximal length of the target, the classical Nyquist conditions in (x, f) space and in (y, θ) space respectively lead one to choose the different sampling intervals Δx, Δf, Δy, and $\Delta\theta$ verifying

$$\Delta x < \frac{c}{2B} , \quad \Delta f < \frac{c}{2L_{\max}} , \quad (40)$$

$$\Delta y < \frac{c}{2f_2 \Delta\theta} , \quad \Delta\theta < \frac{c}{2f_2 L_{\max}} . \quad (41)$$

In the wide angular extent case, the expression (38) cannot be approximated by (39) and its computation is more complex. The different resolutions in range, cross range, frequency, and angle spaces depend on each other and it becomes very difficult to express their mutual dependence analytically. Nevertheless, a numerical analysis can be made by computing the response of a white and isotropic bright point located in $\mathbf{x}_0$. This will be done in the next section using a particular wavelet.

B. A Special Wavelet and Its Analyzing Performances. The chosen wavelet is the product of a Gaussian wavelet in angle space and a minimal Klauder wavelet [11] in k space:

$$\Phi(k, \theta) = k^{2\pi\lambda} e^{-2\pi\lambda} e^{-\theta^2/2\sigma_\theta^2} . \quad (42)$$

The spread of the wavelet in the k variable is related to the real parameter λ by

$$\sigma_k = \frac{1}{\sqrt{4\pi\lambda}} \quad (43)$$

or equivalently in f space by

$$\sigma_f = \frac{c}{4\sqrt{\pi\lambda}} . \quad (44)$$

To illustrate the analyzing performances of this wavelet, we apply it to the study of the following backscattering coefficient:

$$H_{\mathbf{x}_0}(\mathbf{k}) = \frac{e^{-i\mathbf{k}\cdot\mathbf{x}_0}}{k} . \quad (45)$$

This expression can be interpreted as the backscattering coefficient of a bright point situated at $\mathbf{x}_0$ and reflecting evenly for all frequencies and all directions. The factor $1/k$ is necessary to ensure that $H_{\mathbf{x}_0}(\mathbf{k})$ is transformed consistently into $H_{a\mathcal{R}_\phi \mathbf{x}_0 + \mathbf{b}}(\mathbf{k})$ in a change of observers (5) characterized by $(a, \mathcal{R}_\phi, \mathbf{b})$.

The wavelet coefficient of (45) is given according to (15) by

$$C(\mathbf{x} - \mathbf{x}_0, k, \theta) = \int_0^{2\pi} d\theta' \int_0^{\infty} e^{2i\pi\mathbf{k}'\cdot(\mathbf{x}-\mathbf{x}_0)} \times \Phi^*(k'/k, \theta' - \theta) \frac{1}{k} \, dk' . \quad (46)$$

In the small angular extent case, as seen in the previous section, the resolutions in frequency and range spaces are independent of the resolutions in angle and cross-range spaces. The different resolutions σ_x and σ_y of the computed radar images are now given by

$$\sigma_x = \frac{c}{2\sigma_f} , \quad \sigma_y = \frac{c}{2f_2\sigma_\theta} , \quad (47)$$

where σ_f and σ_θ represent the width of the wavelet Φ in frequency and angle, respectively. The interplay between these different resolutions is illustrated on Fig. 3 for a given frequency k and angle of presentation θ. There it can be seen that when λ is increasing, i.e., when the bandwidth σ_f is decreasing, the range resolution σ_x of the radar image becomes poorer. An analogous relation exists between the angular resolution σ_θ and the cross-range resolution σ_y.

In the wide angular extent case the analyzing performances of the wavelet have been studied numerically and the results are displayed in Figs. 4 and 5.

Figure 4 shows the behavior of one bright point for a given frequency width and growing angular extent of the wavelet.

Figure 5 presents the same result for a given wide angular width but different spectral extents of the wavelet. One can remark, especially with Figs. 5(c) and 5(d), that despite the narrow spectral extent of the wavelet, the range resolution is better than in Fig 3(d); this gives an illustration of the coupling between the different resolutions.

C. Examples of Results in a Laboratory Experiment. We now present applications to an experiment made in an anechoic chamber on a model of a missile (Fig. 6) which is 60-cm long and 40-cm wide. The analysis bandwidth is 8.2–12.4 Ghz and the angles vary between −30° and 30°. The samples of the complex backscattering coefficient are collected geometrically in frequency space and regularly in angle space (Fig. 2).

Figures 7–10 represent the results obtained with the computational technique described in Sec. IV for different values of parameters λ and σ_θ in the wavelet (42). In each case we have chosen to display only three images among the $N_f \times N_\theta$ that the algorithm delivers.

Figure 7 represents the two-dimensional radar images obtained for three different frequencies but for a unique direction of illumination. The parameters λ and σ_θ are chosen so as to have good range and cross-range resolutions. One can notice that the three images are not fundamentally different in frequency (the wavelet has a wide bandwidth) with nevertheless a better range resolution at high frequency.

Figure 8 represents the same analysis but with a narrow-

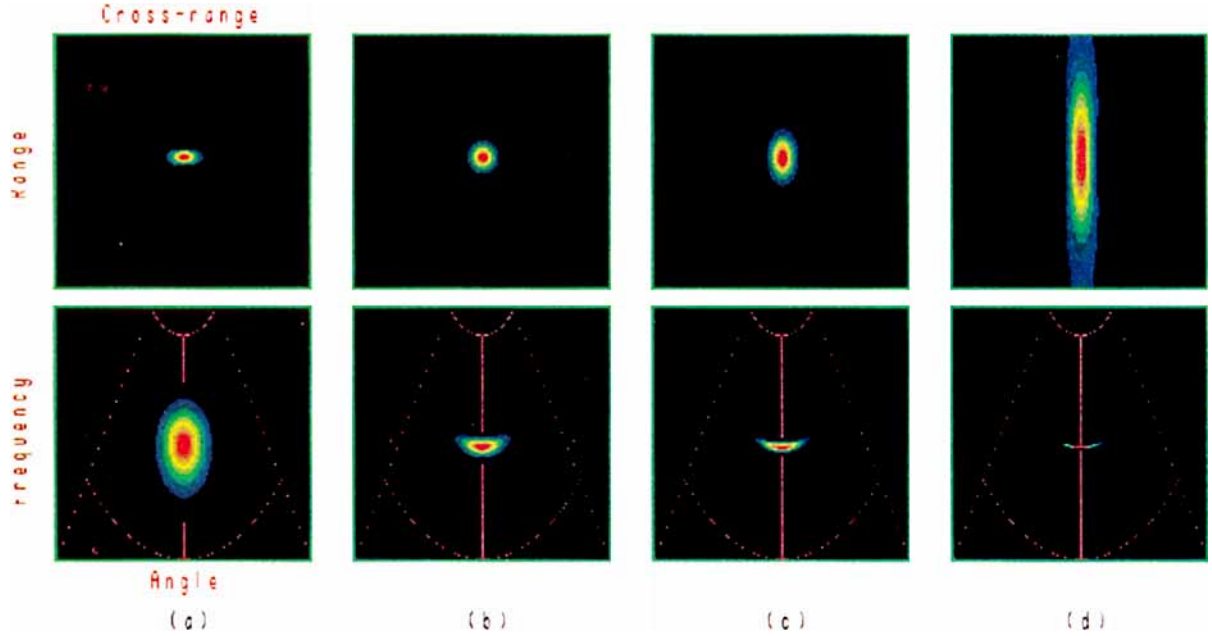

Figure 3. Spatial versus frequency-directivity resolution of a bright point when the bandwidth of the wavelet decreases. Case of narrow angular extent.

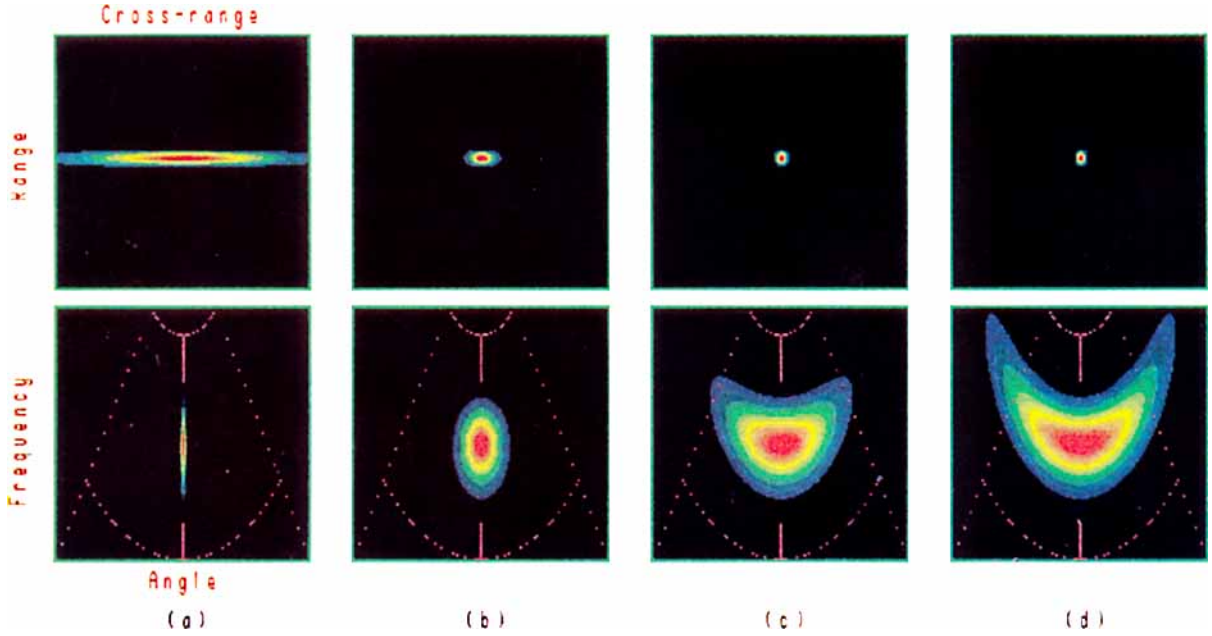

Figure 4. Spatial versus frequency-directivity resolution of a bright point for increasing angular extent of the wavelet.

band wavelet. In this case, the range resolution is not as good as in the previous series but the sensitivity of the pictures to frequency has been increased. These two examples show the duality between good resolutions in range and in frequency.

Figures 9 and 10 show the behavior of the radar images for different angles of target presentation but for the same frequency. The parameters of the wavelet in Fig. 9 are chosen so as to give a good range and cross-range resolutions. One can notice that the right wing has disappeared for $\theta_0 = -25°$ and the left one for $\theta_0 = 25°$.

The image series of Fig. 10 is the result of the search for good resolution in frequency and directivity. The price to pay is clearly a degradation of the spatial localization of the points.

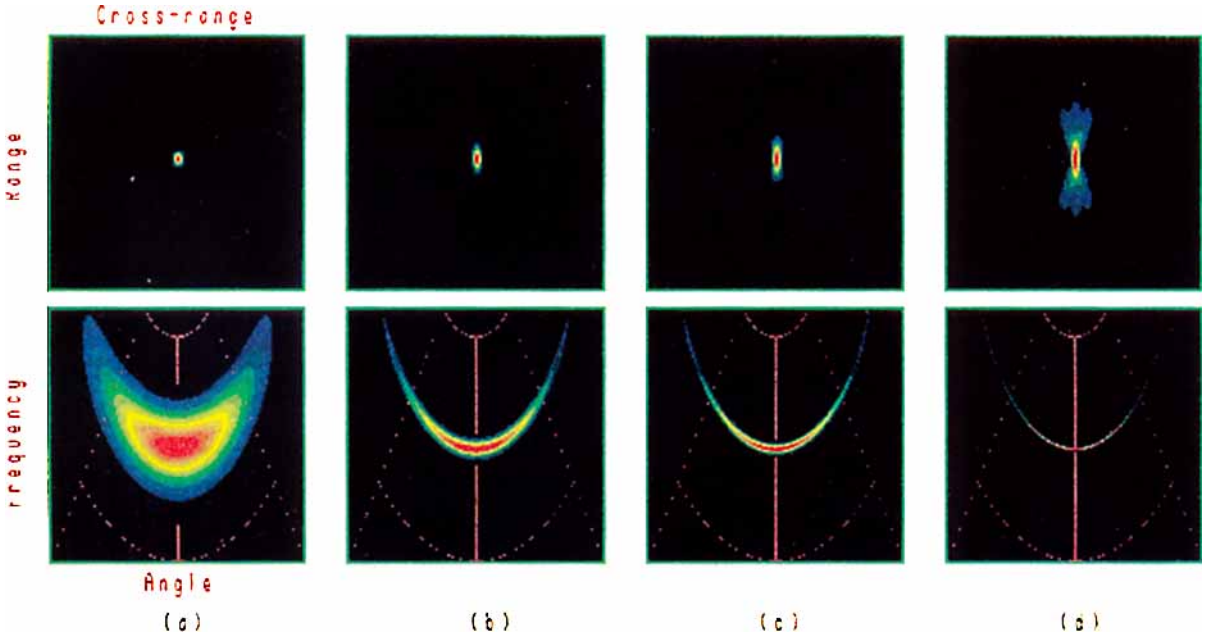

Figure 5. Spatial versus frequency-directivity resolution of a bright point when the bandwidth of the wavelet decreases. Case of wide angular extent.

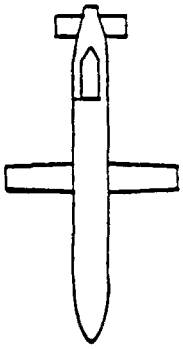

Figure 6. Missile model used for two-dimensional radar imaging.

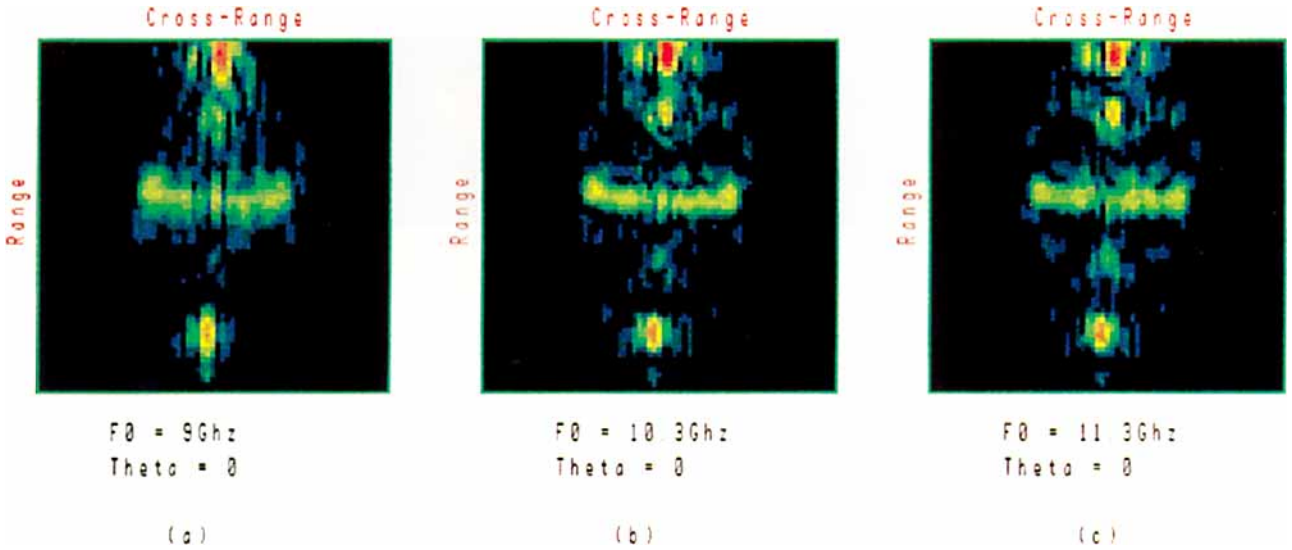

Figure 7. Two-dimensional radar images of a missile. (analysis on [8.2, 12.4] Ghz and [−20, 20] degrees) obtained for large frequency ($\lambda = 10$) and angular ($\sigma_\theta = 20°$) width of the wavelet. The three images are given for the set of parameters ($f = 9$ Ghz, $\theta_0 = 0°$), ($f = 10.3$ Ghz, $\theta_0 = 0°$), and ($f = 11.3$ Ghz, $\theta_0 = 0°$).

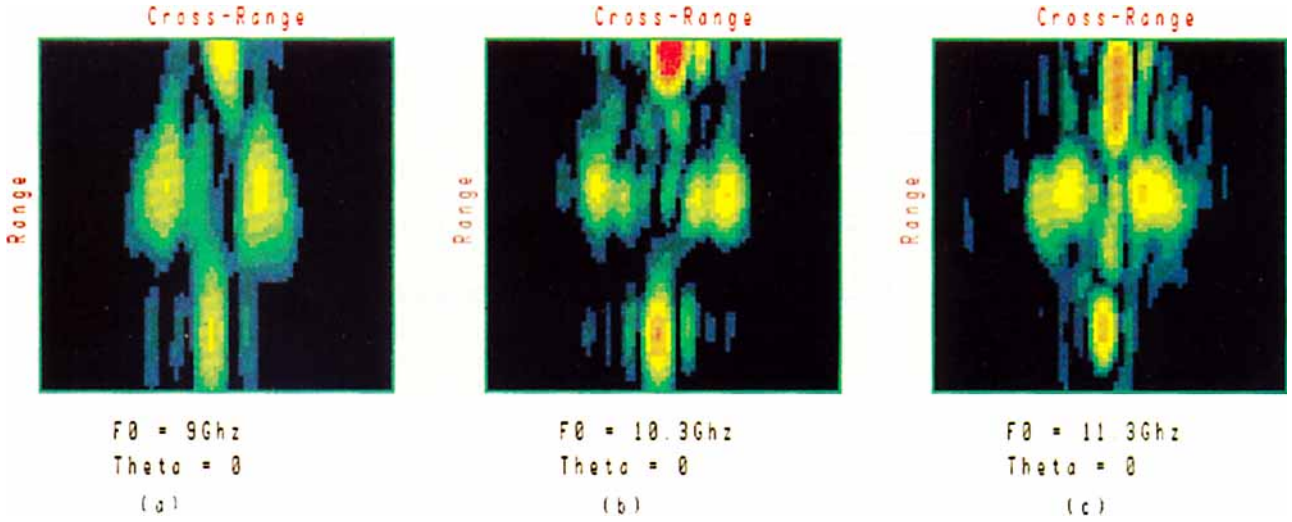

Figure 8. Two-dimensional radar images of a missile (analysis on [8.2, 12.4] Ghz and [−10, 10] degrees) obtained for narrow frequency ($\lambda = 100$) and large angular ($\sigma = 20°$) width of the wavelet. The three images are given for the set of parameters ($f = 9$ Ghz, $\theta_0 = 0°$), ($f = 10.3$ Ghz, $\theta_0 = 0°$), and ($f = 11.3$ Ghz, $\theta_0 = 0°$).

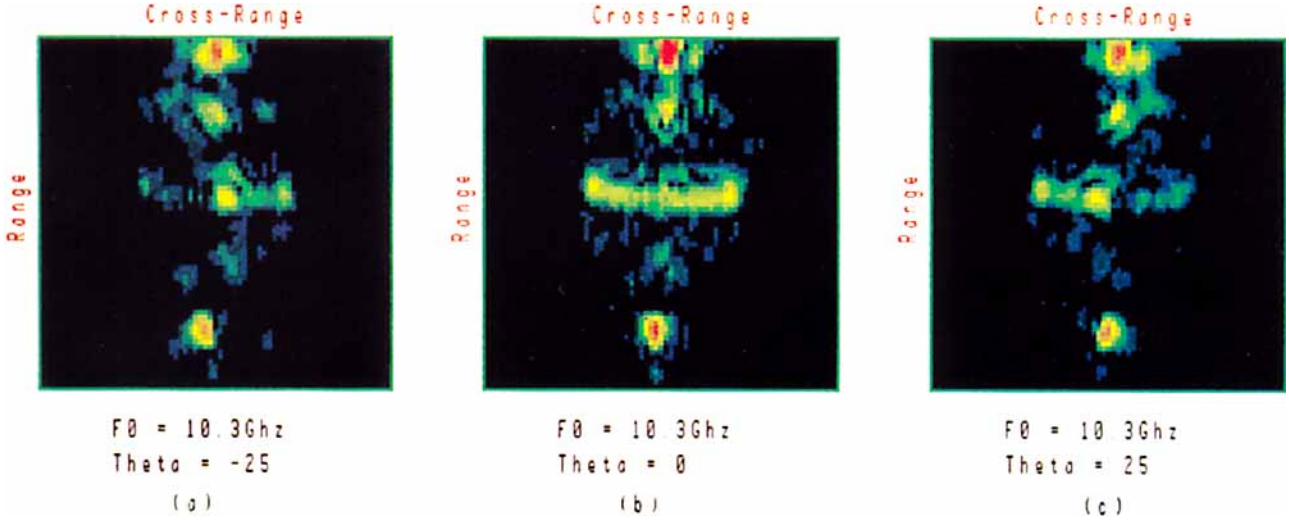

Figure 9. Two-dimensional radar images of a missile (analysis on [8.2, 12.4] Ghz and [−30, 30] degrees) obtained for large frequency ($\lambda = 10$) and angular ($\sigma_\theta = 20°$) width of the wavelet. The three images are given for the set of parameters ($f = 10.3$ Ghz, $\theta_0 = -25°$), ($f = 10.3$ Ghz, $\theta_0 = 0°$), and ($f = 10.3$, $\theta_0 = 25°$).

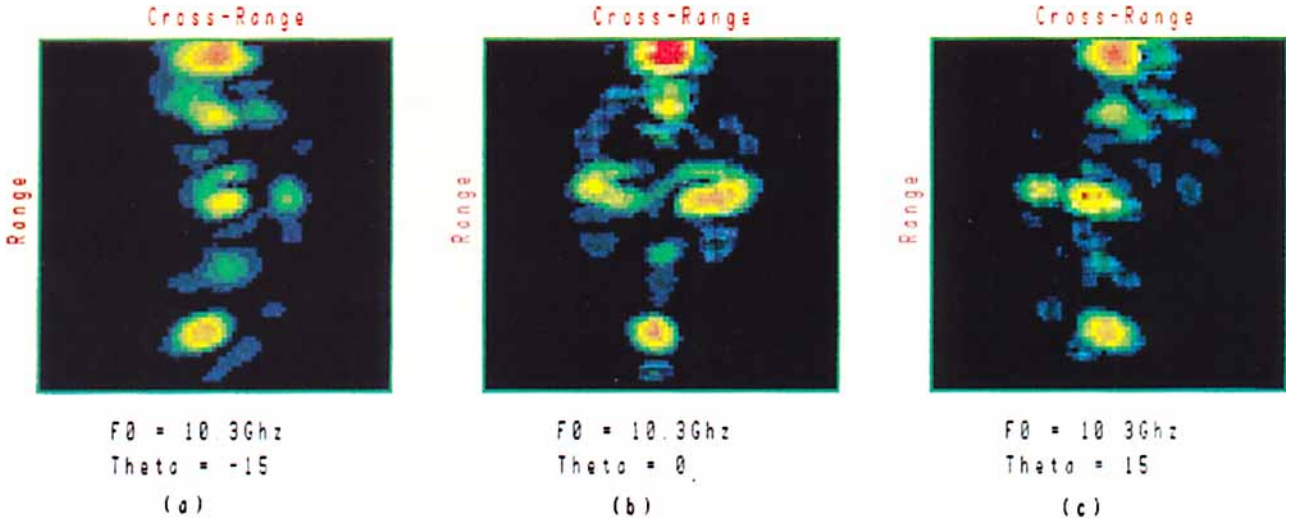

Figure 10. Two-dimensional radar images of a missile (analysis on [8.2, 12.4] Ghz and [−20, 20] degrees) obtained for large frequency ($\lambda = 10$) and narrow angular ($\sigma_\theta = 5°$) width of the wavelet. The three images are given for the set of parameters ($f = 10.3$ Ghz, $\theta_0 = -15°$), ($f = 10.3$ Ghz, $\theta_0 = 0°$), and ($f = 10.3$ Ghz, $\theta_0 = 15°$).

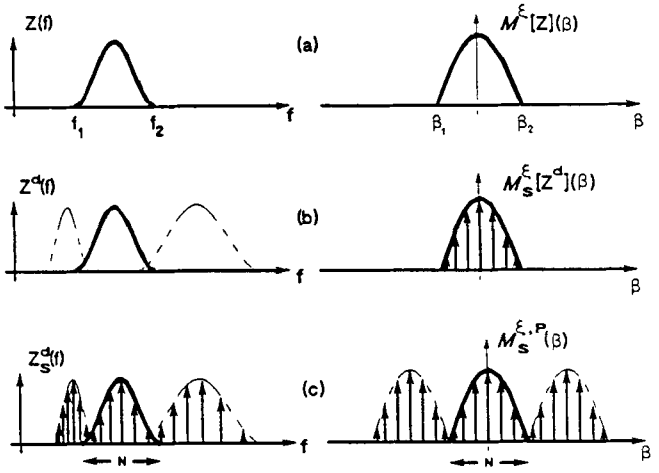

Figure 11. Construction scheme of the discrete Mellin transform. (a) Continuous form of the spectrum $Z(f)$ and its Mellin transform. (b) Dilatocycling of $Z(f)$ with the ratio $Q = f_2/f_1$ and the sampled form of its Mellin transform with rate $1/\ln Q$. (c) Geometric sampling with ratio q ($q^N = Q$) of the dilatocycled form and periodized form with period $1/\ln q$ of the sampled Mellin transform. Identification of the N samples in frequency and Mellin spaces leads to the discrete Mellin transform (A29).

VI. CONCLUSIONS

We have presented a new method to obtain images of a radar target whose backscattering coefficient $H(\mathbf{k})$ has been measured as a function of frequency and orientation for fixed polarizations. The novelty of the procedure lies, on the one hand, in the introduction of a mathematical function of four variables $R(\mathbf{x}, \mathbf{k})$ to represent the spectral image of the target and, on the other hand, in the use of an original method of computation which yields the whole frequency-directivity dependence of each point in a single stroke.

The construction of $R(\mathbf{x}, \mathbf{k})$ has been based on the main requirement that the correspondence between $H(\mathbf{k})$ and $R(\mathbf{x}, \mathbf{k})$ be invariant, in a definite sense, under the similarity group of the plane. We then made use of wavelet analysis associated with this group to obtain an analytical expression of the spectral image in terms of the backscattering function. This expression depends on the choice of the basic wavelet which can be varied at will. As an example, the use of a window-type wavelet in $\mathbf{k}$ space corresponds to introducing frequency-directivity scanning in the usual theory of radar imaging. A more elaborate analysis is provided by the special wavelet (42) which is well localized in $\mathbf{x}$ and $\mathbf{k}$ space and allows a simultaneous study of the dependence of the image on all four variables, with resolutions varying according to the spread of the wavelet.

The computation of the wavelet coefficient entering the expression of $R(\mathbf{x}, \mathbf{k})$ has been carried out by resorting to a special Mellin transform on the radial variable. This transform has been singled out by past work on affine time-frequency distributions and has been made efficient by discretization along with rules of sampling and fast algorithms. An important point in the present application is that the computation uses data in polar format, geometrically distributed in frequency, and no resampling is ever done. It is also worth stressing that the proposed algorithm could be easily implemented on a parallel computer.

To illustrate the connection between the spreading of the basic wavelet and the resolutions of the image we have performed the analysis of a single bright point with wavelets of different spreads. Such a study gives indications for the practical choice of parameters in a real case. Finally, an illustrative application of the method has been given by imaging an actual target.

ACKNOWLEDGMENTS

The authors would like to thank J. C. Castelli at ONERA for his help in the practical applications and the Service Technique des Programmes Aéronautiques for its financial support.

APPENDIX: THE MELLIN TRANSFORM

1. Definition and Properties of the Mellin Transform

a. Definition. The Mellin transform used above was previously introduced in the problem of wide-band time-frequency representation [9] and will be recalled here in that framework. The main interest of this approach is to yield an interpolation of the Mellin variable that permits the establishment of a complete sampling theorem. The lack of such a theorem has often restricted the exploitation of the transform in spite of thorough studies on its discretization [12].

In the following, the frequency variable f will be used and application to Sec. IV will require one only to change from f to k.

Let $Z(f)$ be an analytic signal belonging to $L^2(R^+, f^{2r+1}\,df)$, i.e. with the norm given by

$$(Z, Z) = \int_0^\infty |Z(f)|^2 f^{2r+1}\,df\,, \tag{A1}$$

where r is an arbitrary real number depending on the application.

The Mellin transform of Z is defined by

$$\mathcal{M}^\xi[Z](\beta) = \int_0^\infty Z(f) e^{2i\pi\xi f} \left(\frac{f}{f_0}\right)^{2i\pi\beta} f^r\,df\,, \tag{A2}$$

where f_0 is a reference frequency (chosen arbitrarily) and where ξ is a real parameter.

The inversion formula is

$$Z(f) = \int_{-\infty}^\infty \mathcal{M}^\xi[Z](\beta) e^{-2i\pi\xi f} \left(\frac{f}{f_0}\right)^{-2i\pi\beta} f^{-r-1}\,d\beta\,. \tag{A3}$$

The reference frequency f_0 will usually be equal to 1; as a result the dimensional consistency of the formulas will no longer be manifest.

We now give a list of properties of this transformation. They can be easily established as in the case of the ordinary Mellin transform.

b. Behavior Under Dilations. The basic feature of transformation (A2) appears when performing on the signal a dilation of factor $a > 0$ around a chosen time ξ. This operation, which is defined by

$$Z(f) \rightarrow Z'(f) = a^{r+1} e^{-2i\pi\xi(1-\alpha)f} Z(af)\,, \tag{A4}$$

is represented in Mellin's space as a mere multiplication by a phase:

$$\mathcal{M}^{\xi}[Z](\beta) \rightarrow \mathcal{M}^{\xi}[Z'](\beta) = a^{-2i\pi\beta}\mathcal{M}^{\xi}[Z](\beta) . \quad \text{(A5)}$$

c. Parseval's Formula. If $\mathcal{M}^{\xi}[Z_1]$ and $\mathcal{M}^{\xi}[Z_2]$ are the transforms of Z_1 and Z_2, respectively, then the inner product of Z_1 and Z_2 can be expressed as

$$\int_0^{\infty} Z_1(f)Z_2^*(f)f^{2r+1}\,df = \int_{-\infty}^{\infty} \mathcal{M}^{\xi}[Z_1](\beta)(\mathcal{M}^{\xi})^*[Z_2](\beta)\,d\beta . \quad \text{(A6)}$$

d. Transformation of the Invariant Product. Define a special product noted $\circ$ for two signals Z_1 and Z_2 by

$$(Z_1 \circ Z_2)(f) = f^{r+1}e^{2i\pi\xi f}Z_1(f)Z_2(f) . \quad \text{(A7)}$$

This definition is made to ensure the invariance of the product under transformation (A4). Namely, when both Z_1 and Z_2 are transformed according to (A4), then $Z_1 \circ Z_2$ is transformed in the same way. This is the counterpart of the property of the ordinary product with respect to translations.

The Mellin transform of the product $Z_1 \circ Z_2$ is given by the convolution of the Mellin transforms of Z_1 and Z_2:

$$\mathcal{M}^{\xi}[Z_1 \circ Z_2] = \mathcal{M}^{\xi}[Z_1] * \mathcal{M}^{\xi}[Z_2] . \quad \text{(A8)}$$

e. Transformation of the Multiplicative Convolution. For a given signal $S_1(t)$ the familiar convolution $S_1 * S_2$ of S_1 with any other signal S_2 is the most general linear operation commuting with time translations that can be performed on S_1. Here, since only frequency dilations are available, a new type of convolution has to be introduced. By analogy to the case of translations, the "multiplicative convolution" of Z_1 and Z_2 is defined as the most general linear operation on Z_1 that commutes with dilations (A4). More precisely, suppose a linear operator C_{ξ} is defined in terms of a kernel function $C_{\xi}(f, f')$ according to

$$C_{\xi}[Z_1](f) = \int_0^{\infty} Z_1(f')C_{\xi}(f, f')\,df' . \quad \text{(A9)}$$

Then the requirement that transformation (A4) applied either on Z_1 or $C_{\xi}[Z_1]$ yield the same results implies that

$$a^{r+1}e^{-2i\pi\xi(1-a)f}C_{\xi}[Z_1](af) = \int_0^{\infty} e^{-2i\pi\xi(1-a)f'}Z_1(af')C_{\xi}(f, f')\,df' . \quad \text{(A10)}$$

Using expression (56) together with the fact that relation (57) must be true for any Z_1, we get the following constraint on the kernel

$$C_{\xi}(f, f') \equiv ae^{-2i\pi\xi(1-a)(f-f')}C_{\xi}(af, af') \quad \text{(A11)}$$

valid for any a. The choice $a = f_0/f$ finally leads to

$$C_{\xi}(f, f') = \frac{f_0}{f}\,e^{2i\pi\xi[(f_0/f)-1](f-f')}C_{\xi}\left(f_0, f_0\frac{f'}{f}\right) . \quad \text{(A12)}$$

In the following, the arbitrary reference frequency f_0 will be set equal to 1. Having the general form of a linear operator on Z_1 that commutes with dilations, we may in particular choose $C_{\xi}(1, f)$ to be itself a signal $Z_2(f)$ and define the "multiplicative convolution" of Z_1 and Z_2 as

$$(Z_1 ** Z_2)(f) = \int_0^{\infty} Z_1\left(\frac{f}{f'}\right)Z_2(f')e^{2i\pi\xi[(f/f')+f'-f]}\,\frac{df'}{f'} . \quad \text{(A13)}$$

A straightforward computation shows that the Mellin transform of the multiplicative convolution of the two signals Z_1 and Z_2 is equal to the classical product of their Mellin transforms:

$$\mathcal{M}^{\xi}[Z_1 ** Z_2] = \mathcal{M}^{\xi}[Z_1]\mathcal{M}^{\xi}[Z_2] . \quad \text{(A14)}$$

2. The Discrete Mellin Transform. Discretization of the Mellin transform (A2) is performed along the same lines as discretization of the Fourier transform. It concerns signals with support practically limited, both in f space and in β space. In fact, the discretized Mellin transform will give a relation between N geometrically spaced samples of $Z(f)$ and N arithmetically spaced samples of $\mathcal{M}[Z](\beta)$ [13, 14].

In the development of the discrete Fourier transform, a special role is played by the "Dirac combs" that are invariant by suitable discrete translations. The counterpart here is the geometric sampling distribution defined for a given ratio Q by

$$\Delta^{\xi,r}(f, Q) = \sum_{n=-\infty}^{\infty} Q^{-nr}e^{-2i\pi\xi Q^n}\delta(f - Q^n) . \quad \text{(A15)}$$

This expression is invariant by dilations (A4) of parameter a equal to a power of the ratio Q. The Mellin transform of (A15) is

$$\mathcal{M}^{\xi}[\Delta^{\xi,r}](\beta) = \sum_{n=-\infty}^{\infty} Q^{2i\pi\beta n} , \quad \text{(A16)}$$

which is the Fourier series of the regular Dirac comb:

$$\mathcal{M}^{\xi}[\Delta^{\xi,r}](\beta) = \frac{1}{\ln Q}\sum_{p=-\infty}^{\infty}\delta\left(\beta - \frac{p}{\ln Q}\right) . \quad \text{(A17)}$$

The discretization follows the same steps as in the case of the Fourier transform and will now be detailed.

1. Adjustment of the periodization procedure to the present case leads to the definition of a "dilatocycled" form Z^d of the signal Z by

$$Z^d(f) = \sum_{n=-\infty}^{\infty} Q^{n(r+1)}Z(Q^n f)e^{2i\pi\xi f(Q^n-1)} , \quad \text{(A18)}$$

where $Q = f_2/f_1$ is the ratio of the maximum and minimum frequencies of the support of Z.

Using the Δ distribution (A15) and the muliplicative convolution (A13) makes it possible to rewrite (A18) in the more compact form

$$Z^d(f) = \Delta^{\xi,r}(f, Q) ** Z(f) . \quad \text{(A19)}$$

2. The Mellin transform of Z^d is obtained from (A19) by using (A14) and (A17). It reads

$$\mathcal{M}_S^{\xi}[Z^d](\beta) = \frac{1}{\ln Q} \sum_{p=-\infty}^{\infty} \delta\left(\beta - \frac{p}{\ln Q}\right) \mathcal{M}^{\xi}[Z](\beta) . \tag{A20}$$

The result is a distribution which is characterized by arithmetically spaced samples of $\mathcal{M}^{\xi}[Z](\beta)$.

3. The function $\mathcal{M}_S^{\xi}$ is then periodized in the familiar way with a period $1/\ln q$ which must satisfy the condition

$$\frac{1}{\ln q} > \beta_2 - \beta_1 \tag{A21}$$

in order to avoid aliasing.

According to (A17), this periodization operation can be written:

$$\mathcal{M}_S^{\xi,P}(\beta) = (\mathcal{M}^{\xi}[\Delta^{\cdot,r}(f, q)] * \mathcal{M}_S^{\xi}[Z^d])(\beta) . \tag{A22}$$

It is clear from (A7), (A8), (A15), and (A17) that the inverse Mellin transform of expression (A22), which can be written as

$$Z_S^d(f) = \Delta(f, q) \circ Z^d(f) , \tag{A23}$$

is a distribution built with δ functions at geometrically spaced frequencies. These successive operations are illustrated in Fig. 11.

If the real numbers Q and q appearing in (A20) and (A22) are connected by the relation

$$Q = q^N , \tag{A24}$$

where N is a positive integer, then function $\mathcal{M}_S^{\xi,P}$ defined by (A22) is of periodic impulse type and its inverse Mellin transform is of dilatocyclic [cf. (A18)] impulse type. This distribution can be computed explicitly using (A17) and (A20). The result is

$$\mathcal{M}_S^{\xi,P}(\beta) = \frac{1}{\ln Q} \sum_{m=-\infty}^{\infty} \delta\left(\beta - \frac{m}{\ln Q}\right) \mathcal{M}^{\xi,P}\left(\frac{m}{\ln Q}\right) , \tag{A25}$$

where the periodized Mellin transform $\mathcal{M}^{\xi,P}(\beta)$ with period $1/\ln q = N/\ln Q$ is defined by

$$\mathcal{M}^{\xi,P}(\beta) = \frac{1}{\ln q} \sum_{m=-\infty}^{\infty} \mathcal{M}^{\xi}\left(\beta - \frac{m}{\ln q}\right) . \tag{A26}$$

The discrete Mellin transform formula is obtained by equating $\mathcal{M}_S^{\xi,P}$ given by (A25) and the Mellin transform of Z_S^d which according to (A2) and (A23) can be written as

$$\mathcal{M}_S^{\xi,P}(\beta) = \sum_{n=-\infty}^{\infty} q^{n(r+1)} Z^d(q^n) e^{2i\pi n\beta \ln q} e^{2i\pi\xi q^n} . \tag{A27}$$

Computing the Fourier series coefficient of $\mathcal{M}_S^{\xi,P}$ yields

$$Z^d(q^n) = \frac{q^{-n(r+1)}}{N} \sum_{m=K}^{K+N-1} \mathcal{M}^{\xi,P}\left(\frac{m}{\ln Q}\right) e^{-2i\pi mn/N} e^{-2i\pi\xi q^n} , \tag{A28}$$

where the integer K is given by the integer part of $\beta_1 \ln Q$. Inversion of (A28) is performed using the classical techniques of discrete Fourier transform. This leads to the discrete Mellin transform formula:

$$\mathcal{M}^{\xi,P}\left(\frac{m}{\ln Q}\right) = \sum_{n=M}^{M+N-1} q^{n(r+1)} e^{2i\pi\xi q^n} Z^d(q^n) e^{2i\pi nm/N} , \tag{A29}$$

where the integer M is given by the integer part of $\ln f_1/\ln q$. In fact, since the definition of the periodized $\mathcal{M}^{\xi,P}$ contains a factor $N/\ln Q = 1/\ln q$, the true samples of $\mathcal{M}(\beta)$ are given by $(\ln Q/N)\mathcal{M}^P(m/\ln Q)$. As can be seen on formula (A29), the explicit computation of the discrete Mellin transform may be carried out using any FFT algorithm.

A prerequisite to be able to apply the above formulas to signal analysis, where the signal Z is given with a band B and a duration T, is to find the corresponding support in β of the Mellin transform $\mathcal{M}$ of Z. This is performed by invoking the affine time-frequency representation which yields an interpretation of the β variable in the time-frequency half-plane as labels of the hyperbolas defined by $t = \xi + \beta/f$ [9, 13, 10]. Suppose signal Z is represented by a distribution P whose support lies mainly in a region limited by lines $f = f_1$, $f = f_2$, $t = \xi - T/2$, and $t = \xi + T/2$. Then the two hyperbolas bordering the domain correspond to the extreme points β_1, β_2 of the support of $\mathcal{M}$. Their values are determined by the equations

$$\xi + \frac{T}{2} = \xi + \frac{\beta_2}{f_2} , \tag{A30}$$

$$\xi - \frac{T}{2} = \xi + \frac{\beta_1}{f_2} . \tag{A31}$$

Hence the support of the Mellin transform is characterized by

$$\beta_2 = \frac{f_2 T}{2} , \quad \beta_2 - \beta_1 = f_2 T . \tag{A32}$$

3. Practical Use of the Discretization Formula. Given a signal Z on some frequency band $[f_1, f_2]$ and with duration T, the operations to be performed are the following:

- Find the support $[\beta_1, \beta_2]$ of the Mellin transform of Z using (A32).
- Set $Q = f_2/f_1$.
- Choose the number of samples N in the discretization of the signal such that q defined by

$$\ln q = \frac{\ln Q}{N}$$

verifies

$$\ln q < \beta_2 - \beta_1 .$$

- Apply (A29).

REFERENCES

1. D. L. Mensa, "Radar imaging," *Int. J. Imag. Syst. Technol.* **4**, 148–163 (1992).
2. D. A. Ausherman, A. Kozma, J. L. Walker, H. M. Jones, and E.

C. Poggio, "Developments in radar imaging," *IEEE Trans. Aerospace Electron. Syst.* **20**, 363–398 (1984).
3. D. L. Mensa, *High Resolution Radar Imaging* (Artech House, 1981), Chap. 4.
4. J. Bertrand, P. Bertrand, and J. Ovarlez, "Dimensionalized wavelet transform with application to radar imaging," IEEE-ICASSP (1991).
5. *Wavelets, Time-frequency methods and phase space*, edited by J. M. Combes, A. Grossman, and Ph. Tchamitchian (Springer-Verlag, Berlin, 1989).
6. C. E. Heil and D. F. Walnut, "Continuous and discrete wavelet transforms," *SIAM J. Math. Anal.* **31**, 628–666 (1989).
7. *Wavelets—A Tutorial in Theory and Applications*, edited by C. K. Chui (Academic, New York, 1992).
8. J.-P. Antoine, P. Carrette, R. Murenzi, and B. Piette, "Image analysis with two-dimensional continuous wavelet transform," Signal Process. **31**, 241–272 (1993).
9. J. Bertrand and P. Bertrand, "Représentations temps-fréquence des signaux," *C.R. Acad. Sci. Paris* **299**, 635–638 (1984); "Time-frequency representation of wide-band signals," *Rech. Aerosp.* **1985-5**, 277–283 (1985) (English and French versions).
10. J. Bertrand and P. Bertrand, "Affine time-frequency distributions," in *Time-Frequency Signal Analysis—Methods and Applications*, edited by B. Boashash (Longman-Cheshire, 1991).
11. J. Klauder, in *Functional Integration: Theory and Applications*, edited by J. P. Antoine and E. Tirapegui (Plenum, New York, 1980).
12. M. Bertero, "Sampling theory, resolution limits and inversion methods," in *Inverse Problems in Scattering and Imaging*, edited by M. Bertero and E. R. Pike, Malvern Physics Series (Adam Hilger, Bristol, 1992).
13. J. Bertrand, P. Bertrand, and J. P. Ovarlez, "Discrete Mellin transform for signal analysis," Proc. IEEE ICASSP-90, pp. 1603–1606, 1990.
14. J. P. Ovarlez, "La transformation de Mellin: un outil pour l'analyse des signaux à large bande," doctorate thesis, University Paris 6, 1992.